Supplementary Information for

Deterministic Out-of-Plane Spin Polarization Enabled by Altermagnetic Filtering of Critical Spin Fluctuations

Qian Chen[1, 2,5], Xiaoqian Zhang[1,5], Wenting Lin[1], Wei Jiang[1], Tieyang Zhao[2], Zhenyi Zheng[2], Cheng Zhang[2], Zhaocong Huang[1], Lin Miao[1], Ke Xia[1], Ya Zhai[1], Jingsheng Chen[2,3,4]

[1] Key Laboratory of Quantum Materials and Devices of Ministry of Education, School of Physics, Southeast University, Nanjing, 211189, China

[2] Department of Materials Science and Engineering, National University of Singapore, Singapore, Singapore

[3] Suzhou Research Institute, National University of Singapore, Suzhou, China.

[4] Chongqing Research Institute, National University of Singapore, Chongqing, China. 7

[5] These authors contributed equally: Qian Chen, Xiaoqian Zhang

Email: kexia@seu.edu.cn, yazhai@seu.edu.cn, msecj@nus.edu.sg

Content

S1 Structure and Magnetic Characterizations

As shown in Fig. S1a, the RHEED patterns of both $CrTe_2$ and CrSb films display stripe-like features with a clear "1 × 1" periodicity, indicating the successful formation of two-dimensional crystalline layers. When a monolayer of CrSb is deposited atop $CrTe_2$, the first-order diffraction spots shift closer together, reflecting the slightly larger in-plane lattice constant of CrSb relative to $CrTe_2$. From these diffraction data, the in-plane lattice constants are estimated to be 4.07 Å for CrSb and 3.91 Å for $CrTe_2$.

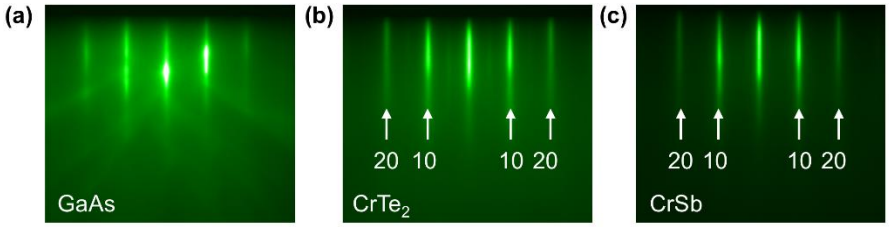

FIG. S1 In-situ RHEED patterns of $CrTe_2$ and CrSb films on GaAs (0001).

The temperature-dependent magnetization of $CrTe_2$ is shown in Fig. S2, revealing a Curie temperature of approximately 305 K.

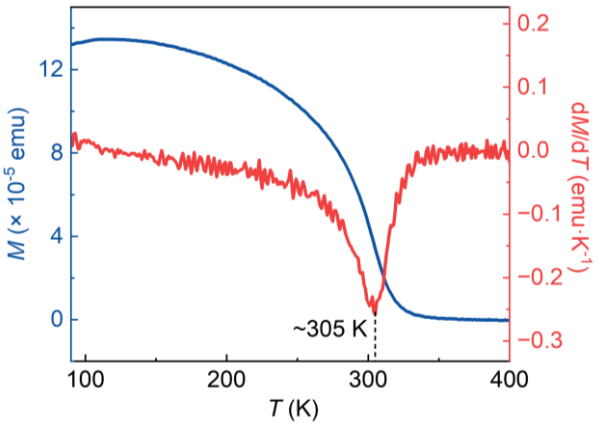

FIG. S2 Temperature dependence of the magnetization of $CrTe_2$.

The magnetic hysteresis loop of the Fe film is presented in Fig. S3, demonstrating that an in-plane magnetic field of 1000 Oe is adequate to achieve its saturation.

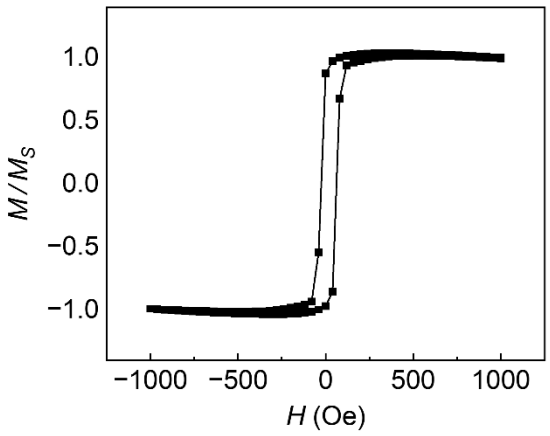

FIG. S3 Room-temperature magnetic hysteresis loop of the Fe film.

S2 Derivation of the Angular Dependence of Third-Order Hall Resistance

With an alternating current $\overrightarrow{I_{ac}} = I_0\, sin(\omega t)\, \hat{x}$, the Hall voltage can be expressed as

$$V_{xy} = R_{xy} I_0 \sin \omega t$$

R_{xy} is the Hall resistance consists of mainly the AHE and PHE,

$$R_{xy} = R_A m_z + R_P^0 m_x m_y$$

$$= R_A \cos\theta + R_P \sin 2\varphi \sin^2\theta$$

R_A and R_P are AHE and PHE coefficients respectively. After Taylor expansion of $\Delta\theta$ and $\Delta\varphi$ related terms to the second-order small quantities, the Hall voltage is expressed as:

$$V_y \approx \Big[R_A\Big(\cos\theta - \sin\theta\cdot\Delta\theta - \frac{\cos\theta}{2}\cdot\Delta\theta^2\Big) + R_P(\sin2\varphi + 2\cos2\varphi\cdot\Delta\varphi - 2\sin2\varphi\cdot\Delta\varphi^2)(\sin^2\theta + \sin 2\theta\cdot\Delta\theta + \cos 2\theta\cdot\Delta\theta^2)\Big]\cdot I_0 \sin\omega t$$

In *xy*-plane, it can be simplified as

$$V_y \approx [-R_A\cdot\Delta\theta + R_P(\sin2\varphi + 2\cos2\varphi\cdot\Delta\varphi - 2\sin2\varphi\cdot\Delta\varphi^2)(1-\Delta\theta^2)]\cdot I_0\sin\omega t$$
$$\approx [-R_A\cdot\Delta\theta + R_P\sin2\varphi + 2R_P\cos2\varphi\cdot\Delta\varphi - 2R_P\sin2\varphi\cdot\Delta\varphi^2 - R_P\cdot\sin2\varphi\cdot\Delta\theta^2]\cdot I_0\sin\omega t$$

Here, $\Delta\theta$and $\Delta\phi$can be obtained by solving the equilibrium equations under the effective field induced by the spin torque, and are given by[1]

$$\Delta\theta = \frac{\cos\theta\,(\Delta H_x\cos\varphi + \Delta H_y\sin\varphi) - \Delta H_z\sin\theta}{H_k\cos2\theta + H}$$

$$\Delta\varphi = \frac{-\Delta H_x\sin\varphi + \Delta H_y\cos\varphi}{H}$$

The effective field $\overrightarrow{\Delta H}$ originates from the spin torque. For nonlinear systems, it can be expressed as

$$\overrightarrow{H_{FL}} = (H_{FL}\sin\omega t + H_{NLFL}\sin^2\omega t)\cdot\hat{\sigma}$$

$$\overrightarrow{H_{DL}} = (H_{DL}\sin\omega t + H_{DLFL}\sin^2\omega t)\cdot(\hat{m}\times\hat{\sigma})$$

where $H_{DL(FL)}$ and $H_{NLDL(NLFL)}$ denote the linear and nonlinear damping-like (field-like) spin torque effective fields, respectively. $\hat{\sigma} = (a, b, c)$ denotes the spin polarization direction. The total effective field is then given by

$$\overrightarrow{\Delta H} = \overrightarrow{H_{FL}} + \overrightarrow{H_{DL}}$$

$$= \begin{pmatrix} \left(H_{DL}\sin\omega t + H_{DL}^{'}\sin^2\omega t\right)(\sin\varphi\sin\theta\cdot c - \cos\theta\cdot b) + \left(H_{FL}\sin\omega t + H_{FL}^{'}\sin^2\omega t\right)\cdot a \\ \left(H_{DL}\sin\omega t + H_{DL}^{'}\sin^2\omega t\right)(\cos\theta\cdot a - \cos\varphi\sin\theta\cdot c) + \left(H_{FL}\sin\omega t + H_{FL}^{'}\sin^2\omega t\right)\cdot b \\ \left(H_{DL}\sin\omega t + H_{DL}^{'}\sin^2\omega t\right)(\cos\varphi\sin\theta\cdot b - \sin\varphi\sin\theta\cdot a) + \left(H_{FL}\sin\omega t + H_{FL}^{'}\sin^2\omega t\right)\cdot c \end{pmatrix}$$

For $\hat{\sigma} = (1,0,0)$, we have

$$\begin{aligned} V_y \approx \Bigg[&\frac{R_A}{H_k - H}(H_{DL}\sin\omega t + H_{NLDL}\sin^2\omega t)\sin\varphi + R_P\sin2\varphi \\ &- \frac{2R_P\cos2\varphi}{H}(H_{FL}\sin\omega t + H_{NLFL}\sin^2\omega t)\sin\varphi \\ &- \frac{2R_P\sin2\varphi}{H^2}(H_{FL}\sin\omega t + H_{NLFL}\sin^2\omega t)^2\sin^2\varphi \\ &- \frac{R_P\cdot\sin2\varphi}{(-H_k + H)^2}(H_{DL}\sin\omega t + H_{NLDL}\sin^2\omega t)^2\sin^2\varphi\Bigg]\cdot I_0\sin\omega t \end{aligned}$$

Therefore,

$$\begin{aligned} {R_y}^{3\omega} = \frac{{V_y}^{3\omega}}{I_0} \approx &-\frac{1}{4}\cdot\frac{R_A H_{NLDL}}{H_k - H}\sin\varphi + \frac{1}{2}\cdot\frac{R_P H_{NLFL}}{H}\cos2\varphi\sin\varphi + \frac{1}{4} \\ &\cdot\left[\frac{2R_P{H_{FL}}^2}{H^2} + \frac{R_P{H_{NLDL}}^2}{(-H_k + H)^2}\right]\sin2\varphi\sin^2\varphi \end{aligned}$$

For $\hat{\sigma} = (0,1,0)$, we have

$$\begin{aligned} V_y \approx \Bigg[&\frac{R_A}{-H_k + H}(H_{DL}\sin\omega t + H_{NLDL}\sin^2\omega t)\cos\varphi + R_P\sin2\varphi \\ &+ \frac{2R_P}{H}(H_{FL}\sin\omega t + H_{NLFL}\sin^2\omega t)\cos2\varphi\cos\varphi \\ &- \frac{2R_P}{H^2}(H_{FL}\sin\omega t + H_{NLFL}\sin^2\omega t)^2\sin2\varphi\cos^2\varphi \\ &- \frac{R_P(H_{DL}\sin\omega t + H_{NLDL}\sin^2\omega t)^2}{(-H_k + H)^2}\cdot\sin2\varphi\cos^2\varphi\Bigg]\cdot I_0\sin\omega t \end{aligned}$$

Therefore

$$\begin{aligned} {R_y}^{3\omega} \approx &-\frac{1}{4}\cdot\frac{R_A H_{NLDL}}{-H_k + H}\cos\varphi - \frac{1}{2}\cdot\frac{R_P H_{NLFL}}{H}\cos2\varphi\cos\varphi + \frac{1}{4} \\ &\cdot\left[\frac{2R_P{H_{FL}}^2}{H^2} + \frac{R_P{H_{DL}}^2}{(-H_k + H)^2}\right]\sin2\varphi\cos^2\varphi \end{aligned}$$

For $\hat{\sigma} = (0,0,1)$, we have

$$V_y \approx \left[\frac{R_A}{-H_k + H}(H_{FL}\sin\omega t + H_{NLFL}\sin^2\omega t) + R_P\sin 2\varphi \right.$$
$$- \frac{2R_P}{H}(H_{DL}\sin\omega t + H_{NLDL}\sin^2\omega t)\cos 2\varphi$$
$$- \frac{2R_P}{H^2}(H_{DL}\sin\omega t + H_{NLDL}\sin^2\omega t)^2\sin 2\varphi$$
$$\left. - \frac{R_P(H_{FL}\sin\omega t + H_{NLFL}\sin^2\omega t)^2}{(H_k - H)^2}\cdot\sin 2\varphi\right]\cdot I_0\sin\omega t$$

Therefore

$$R_y{}^{3\omega} \approx -\frac{1}{4}\cdot\frac{R_A H_{NLFL}}{-H_k + H} + \frac{1}{2}\cdot\frac{R_P H_{NLDL}}{H}\cos 2\varphi + \frac{1}{4}\cdot\left[\frac{2R_P {H_{DL}}^2}{H^2} + \frac{R_P {H_{FL}}^2}{(H_k - H)^2}\right]\sin 2\varphi$$

The derivation of the longitudinal third-order magnetoresistance follows a similar procedure.

S3 Thermal Effects on Third-Order Magnetoresistances

The thermal effect is mainly manifested as the influence of the Spin Seebeck Effect (SSE) and Spin Nernst Effect (SNE) on the second-order resistance being transmitted to the third order. The second-order resistance terms generated by SSE and SNE can be expressed as:

$$R_x^{2\omega} = k_{\nabla T}\frac{l}{w}I_0\sin\varphi$$

$$R_y^{2\omega} = k_{\nabla T}I_0\cos\varphi$$

$k_{\nabla T}$ is the thermal resistance coefficient related to SSE and SNE, and $\frac{l}{w}$ denotes the length-to-width ratio of the core device.

$$V_y = k_{\nabla T}I_0\cos(\varphi + \Delta\varphi)\cdot I_0\cos(2\omega t) = k_{\nabla T}{I_0}^2\cos(\varphi + \Delta\varphi) - 2k_{\nabla T}{I_0}^2\cos(\varphi + \Delta\varphi)\sin^2(\omega t)$$

Which can be further simplified as

$$V_y = k_{\nabla T}{I_0}^2\left(\cos\varphi - \sin\varphi\cdot\Delta\varphi - \frac{\cos\varphi}{2}\cdot\Delta\varphi^2\right)$$
$$- 2k_{\nabla T}{I_0}^2\left(\cos\varphi - \sin\varphi\cdot\Delta\varphi - \frac{\cos\varphi}{2}\cdot\Delta\varphi^2\right)\sin^2(\omega t)$$

Extracted thermal effects on the third harmonic responses are summarized as Table S1.

Table S1 Thermal Effects on the Third-Harmonic Signals

	$R_y^{3\omega}$	$R_x^{3\omega}$
$\hat{\boldsymbol{\sigma}}_{\boldsymbol{x}}$	$\frac{k_{\nabla T} I_0 \cdot H_{FL}}{2H} \sin^2\varphi$ $+\frac{k_{\nabla T} I_0 \cdot H_{FL} \cdot H_{NLFL}}{4H^2} \cos\varphi \sin^2\varphi$	$-k_{\nabla T} \frac{l H_{FL}}{2wH} I_0 \cos\varphi \sin\varphi$ $+ k_{\nabla T} \frac{l \cdot H_{FL} \cdot H_{NLFL}}{4wH^2} I_0 \sin^3\varphi$
$\hat{\boldsymbol{\sigma}}_{\boldsymbol{y}}$	$-\frac{k_{\nabla T} I_0 \cdot H_{FL}}{2H} \sin\varphi \cos\varphi$ $+\frac{k_{\nabla T} I_0 \cdot H_{FL} \cdot H_{NLFL}}{4H^2} \cos^3\varphi$	$k_{\nabla T} \frac{l H_{FL}}{2wH} I_0 \cos^2\varphi$ $+ k_{\nabla T} \frac{l \cdot H_{FL} \cdot H_{NLFL}}{4wH^2} I_0 \sin\varphi \cos^2\varphi$
$\hat{\boldsymbol{\sigma}}_{\boldsymbol{z}}$	$\frac{k_{\nabla T} I_0 \cdot H_{DL}}{2H} \sin\varphi$ $+\frac{k_{\nabla T} I_0 \cdot H_{DL} \cdot H_{NLDL}}{4H^2} \cos\varphi$	$-k_{\nabla T} \frac{l \cdot H_{DL}}{2wH} I_0 \cos\varphi$ $+ k_{\nabla T} \frac{l \cdot H_{DL} \cdot H_{NLDL}}{4wH^2} I_0 \sin\varphi$

S4 Extraction of R_A and R_P from First-Harmonic Hall Resistances

The parameters R_P and R_A can be independently extracted by fitting the angular dependence of the first-harmonic Hall resistance measured in the xy- and yz-planes, respectively.

As shown in Fig. S4(a), in the xy-plane configuration, the first-harmonic Hall resistance $R_{xy}^{1\omega}$ follows

$$R_{xy}^{1\omega} = R_P \sin 2\varphi$$

from which a fitting yield $R_P = 52.61 \pm 0.80$ mΩ.

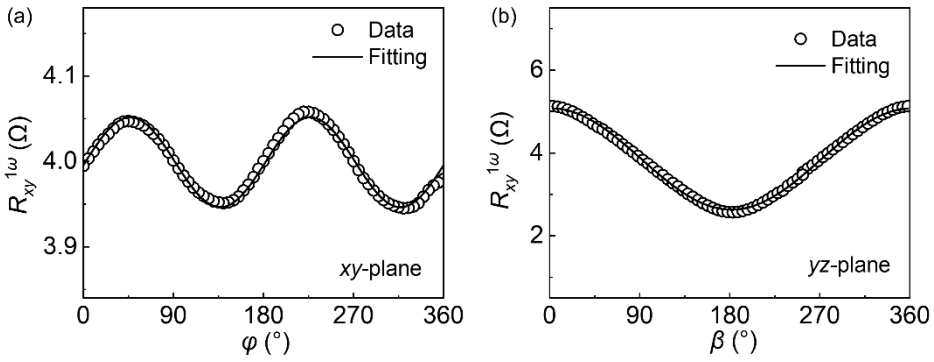

FIG. S4 (a) Angular dependence of the first-harmonic Hall resistance $R_{xy}^{1\omega}$ measured with the magnetic field rotated in the xy-plane. (b) Angular dependence of $R_{xy}^{1\omega}$ measured with the magnetic field rotated in the yz-plane.

As shown in Fig. S4(b), when the magnetic field is rotated in the yz-plane, the angular dependence of $R_{xy}^{1\omega}$ can be described by

$$R_{xy}^{1\omega} = R_A \cos\theta$$

Accordingly, the fitting yields $R_A = 1219.17 \pm 5.03$ mΩ.

S5 Longitudinal magnetoresistance measured in the *xy*-Plane

The first- and third-harmonic longitudinal magnetoresistance measured in the xy-plane are shown in Fig. S5(a) and (b), respectively. We attempted to fit the third-harmonic longitudinal resistance $R_x^{3\omega}$ using the angular dependence expressions summarized in Table 1 and Table S1. However, it was found that the contributions arising from nonlinear spin–orbit torques cannot be unambiguously separated from those originating from thermoelectric effects in this configuration.

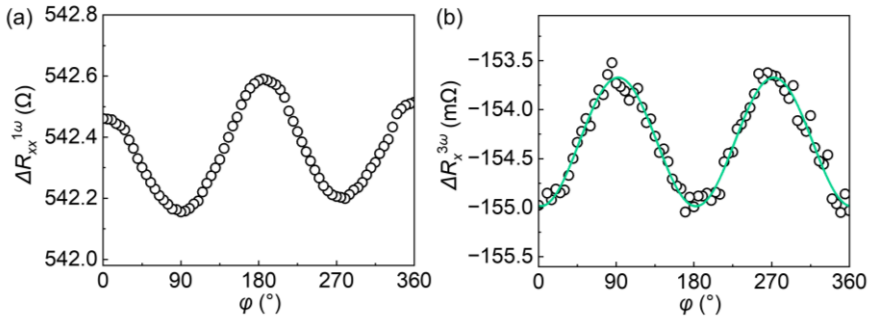

FIG. S5 (a) First-harmonic longitudinal magnetoresistance $R_{xx}^{1\omega}$ measured with the magnetic field rotated in the xy-plane. (b) Third-harmonic longitudinal magnetoresistance $R_x^{3\omega}$ measured under the same rotation configuration. The solid line shows the fitting curve with the coexistence of nonlinear spin-orbit torque and thermoelectric contributions.

S6 Third-Harmonic Hall Response of the Fe/Te Control Sample

Third-harmonic Hall measurements were performed on the control sample consisting of an 8-nm Fe layer capped with Te, and the results are shown in Fig. S6. At current amplitudes comparable to those applied to the $CrTe_2$/CrSb/Fe samples, the third-harmonic Hall resistance is barely detectable. Upon further increasing the current up to 2 mA, a finite $R_y^{3\omega}$ signal emerges, which is dominated by thermoelectric effects. Even at higher current levels, no discernible contribution attributable to nonlinear spin-orbit torques can be identified.

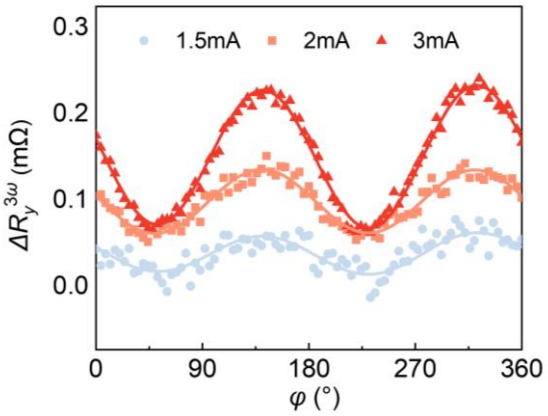

FIG. S6 Third-harmonic Hall resistance $R_y^{3\omega}$ of the Fe/Te control sample measured under various applied current amplitudes. The data indicate that the observed $R_y^{3\omega}$ signal at higher currents is dominated by thermoelectric effects.

S7 Third-Harmonic Hall Response of the $CrTe_2$/Fe/Te Control Sample

Third-harmonic Hall measurements were also carried out on the $CrTe_2$/Fe control sample capped with Te, and the results are shown in Fig. S7(a). Measurements were performed for different crystallographic orientations. At current amplitudes comparable to those applied to the $CrTe_2$/CrSb/Fe samples, the third-harmonic Hall signal is nearly absent. As the current is further increased, a finite $R_y^{3\omega}$ signal emerges, which is dominated by thermoelectric effects. Similarly, no discernible contribution from nonlinear spin–orbit torques is observed, as shown in Fig. S7(b) and Fig. S7(c).

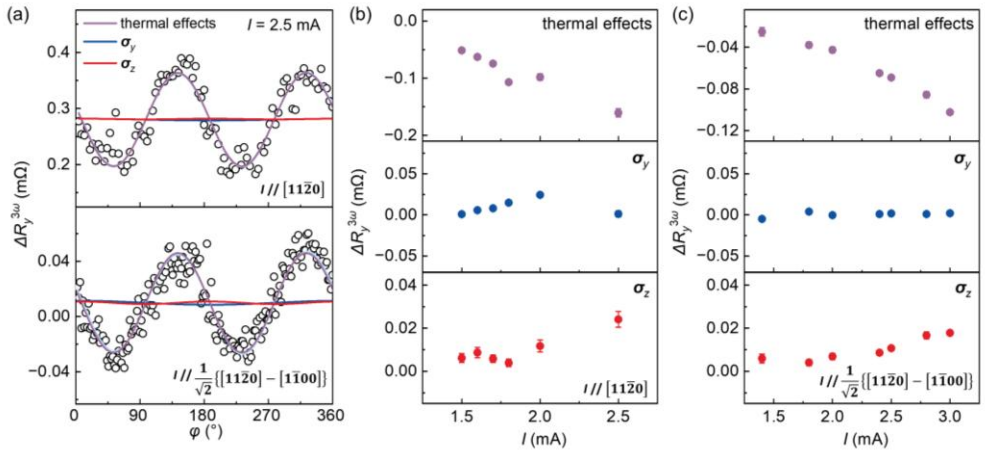

FIG. S7 (a) Third-harmonic Hall resistance $R_y^{3\omega}$ of the $CrTe_2$/Fe/Te control sample measured at 2.5 mA. (b,c) Extracted $R_y^{3\omega}$ measured along two different crystallographic orientations, decomposed into contributions from different sources.

S8 Comparisons of Spin Torque–Equivalent Fields in Conventional Linear Systems

Table S1 Spin torque–equivalent fields in linear systems

Structures	$H_{DL,y}$ (10^{-10} Oe·A^{-1}m^2)	$H_{DL,z}$ (10^{-10} Oe·A^{-1}m^2)	Ref.
Pt/Co	1.7	-	Ref. [2]
Pt/[Co/Ni]$_2$	4	-	Ref. [3]
Pt/Co	6.9	-	Ref. [4]
Pt/LSMO	2.5	-	Ref. [5]
Ta/CoFeB	2	-	Ref. [6]
Ta/CoFeB	4	-	Ref. [7]
W/CoFeB	3	-	Ref. [8]
W/CoFeB	1.25	-	Ref. [9]
CuPt/CoPt	2.2	0.6	Ref. [10]
CuPt/CoPt	0.9	0.4	Ref. [11]
Pt/Co/Ta	5	0.2	Ref. [12]
$WTe_2/Fe_{2.78}GeTe_2$	-	8	Ref. [13]

S9 Current-Induced Temperature Variation in the Device

We quantified the temperature rise of the device induced by the applied current. First, at 300 K, the device resistance was measured as a function of current within the experimental range, as shown in Fig. S8(a). In parallel, the temperature dependence of the device resistance was calibrated using a small probing current of 40 μA (~2.4×10^8 A/m^2), as shown in Fig. S8(b). By correlating the resistance values obtained at different currents with the temperature calibration curve, the actual device temperature as a function of applied current was determined, as presented in Fig. S8(c). These measurements indicate that, under the experimental current conditions, the device temperature increases by no more than ~2 K.

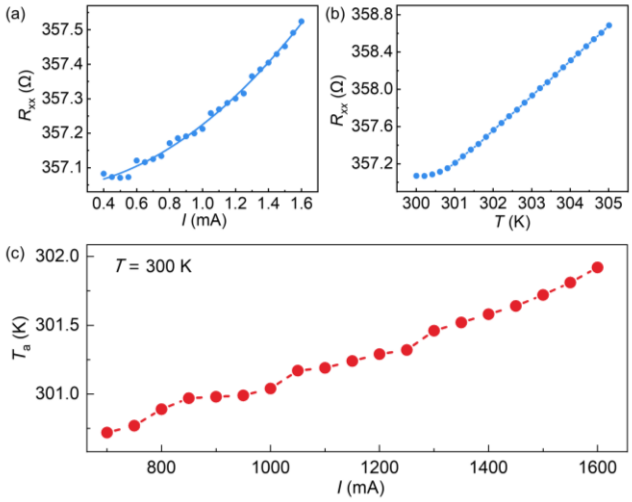

FIG. S8 (a) Measured device resistance as a function of applied current at 300 K within the experimental range used in this study. (b) Temperature dependence of the device resistance. (c) Estimated actual device temperature as a function of applied current

S10 Second-Harmonic Responses and Their Dependence on the Magnetic Field

Second-harmonic Hall and longitudinal resistance measurements were performed on the $CrTe_2$/CrSb/Fe sample. The angular dependencies of $R_y^{2\omega}$ and $R_x^{2\omega}$ are shown in Fig. S9(a) and (c), respectively, while their variations with the applied magnetic field are presented in Fig. S9(b) and (d). Both $R_y^{2\omega}$ and $R_x^{2\omega}$ increase in amplitude with increasing magnetic field, indicating that they cannot be attributed to linear spin-current-induced spin-orbit torques, but instead arise from nonlinear effects[14,15].

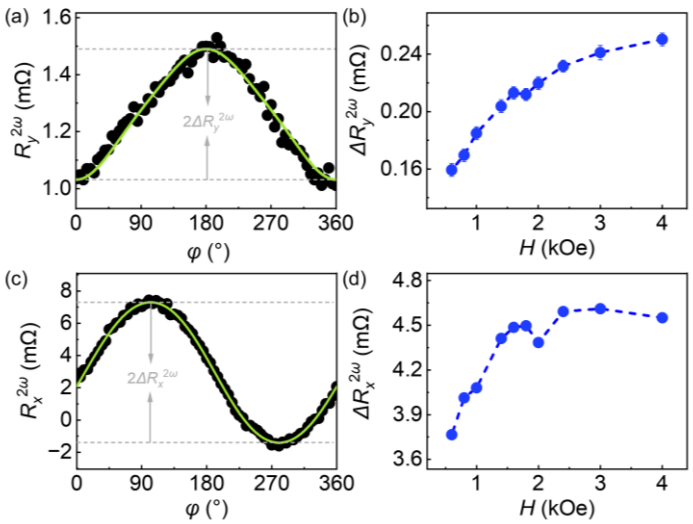

FIG. S9 (a,c) Angular dependence of $R_y^{2\omega}$ and $R_x^{2\omega}$, respectively. (b,d) Magnetic-field dependence of the corresponding second-harmonic signals of $R_y^{2\omega}$ and $R_x^{2\omega}$, respectively.

S11 Third-Harmonic Hall Resistances Measured in the *yz*-Plane

The first-, second-, and third-harmonic Hall and longitudinal resistances of the $CrTe_2$/CrSb/Fe sample measured with the magnetic field rotated in the yz-plane are shown in Fig. S11. A clear third-harmonic magnetoresistance response is also observed in this measurement configuration.

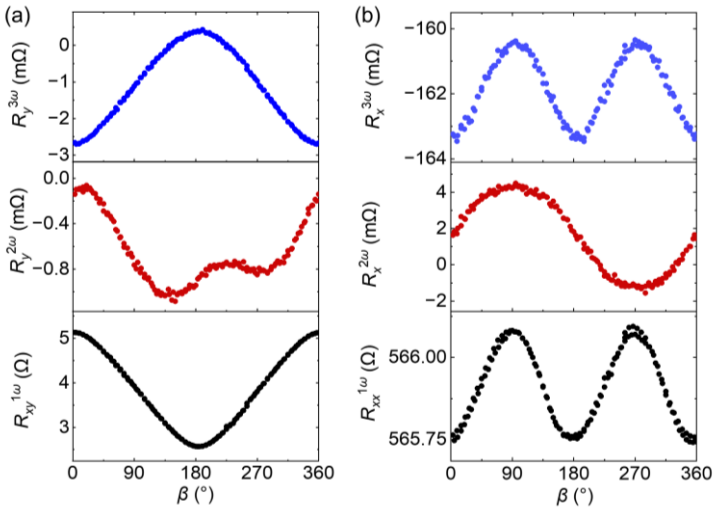

FIG. S10 First-, second-, and third-harmonic (a) Hall and (b) longitudinal resistances measured with the magnetic field rotated in the yz-plane.

References

1 Hayashi, M., Kim, J., Yamanouchi, M. & Ohno, H. Quantitative characterization of the spin-orbit torque using harmonic Hall voltage measurements. *Phys. Rev. B* **89**, 144425 (2014).

2 Liu, L., Lee, O. J., Gudmundsen, T. J., Ralph, D. C. & Buhrman, R. A. Current-Induced Switching of Perpendicularly Magnetized Magnetic Layers Using Spin Torque from the Spin Hall Effect. *Phys. Rev. Lett.* **109**, 096602 (2012).

3 Yu, J. *et al.* Long spin coherence length and bulk-like spin–orbit torque in ferrimagnetic multilayers. *Nat. Mater.* **18**, 29-34 (2019).

4 Garello, K. *et al.* Symmetry and magnitude of spin–orbit torques in ferromagnetic heterostructures. *Nat. Nanotechnol.* **8**, 587-593 (2013).

5 Chen, H. *et al.* Spin-Orbit Torque Switching of Magnetization in Ultra-Thick Ferromagnetic Layers. *Adv. Funct. Mater.* **34**, 2403107 (2024).

6 Schulz, T. *et al.* Effective field analysis using the full angular spin-orbit torque magnetometry dependence. *Phys. Rev. B* **95**, 224409 (2017).

7 Liu, L. *et al.* Spin-Torque Switching with the Giant Spin Hall Effect of Tantalum. *Science* **336**, 555-558 (2012).

8 Xu, J. & Chien, C. L. Voltage-controlled spin–orbit torque switching in W/CoFeB/MgO. *Appl. Phys. Lett.* **118**, 052409 (2021).

9 Cierpiał, M. *et al.* Spin-orbit-torque-induced magnetization switching in α-W-based

magnetic tunnel junction. *J Phys. D: Appl. Phys.* **59**, 025007 (2026).

10 Zhao, T. *et al.* Enhancement of Out-of-Plane Spin–Orbit Torque by Interfacial Modification. *Adv. Mater.* **35**, 2208954 (2023).

11 Liu, L. *et al.* Symmetry-dependent field-free switching of perpendicular magnetization. *Nat. Nanotechnol.* **16**, 277-282 (2021).

12 Zeng, G. *et al.* Deterministic field-free switching of perpendicular magnetization via out-of-plane spin polarization induced by in-plane asymmetry in Ta heterostructures. *Phys. Rev. Appl.* **24**, 044086 (2025).

13 Kao, I. H. *et al.* Deterministic switching of a perpendicularly polarized magnet using unconventional spin–orbit torques in WTe_2. *Nat. Mater.* **21**, 1029-1034 (2022).

14 He, P. *et al.* Nonlinear Planar Hall Effect. *Phys. Rev. Lett.* **123**, 016801 (2019).

15 Kozuka, Y. *et al.* Observation of Nonlinear Spin-Charge Conversion in the Thin Film of Nominally Centrosymmetric Dirac Semimetal $SrIrO_3$ at Room Temperature. *Phys. Rev. Lett.* **126**, 236801 (2021).